

DSF-24/2006, IFIC/06-21, MPP-2006-89

# Ultra High Energy Neutrinos in the Mediterranean: detecting $\nu_\tau$ and $\nu_\mu$ with a $\text{km}^3$ Telescope

**A. Cuoco<sup>1</sup>, G. Mangano<sup>1</sup>, G. Miele<sup>1</sup>, S. Pastor<sup>2</sup>,  
L. Perrone<sup>3</sup>, O. Pisanti<sup>1</sup>, and P.D. Serpico<sup>4</sup>**

<sup>1</sup> Dipartimento di Scienze Fisiche, Università di Napoli *Federico II* and INFN  
Sezione di Napoli, Complesso Universitario di Monte S. Angelo, Via Cinthia, I-80126  
Napoli, Italy.

<sup>2</sup> Instituto de Física Corpuscular (CSIC-Universitat de València), Ed. Institutos de  
Investigación, Apdo. 22085, E-46071 València, Spain.

<sup>3</sup> Dipartimento di Ingegneria dell'Innovazione, Università di Lecce and INFN Sezione  
di Lecce, Via per Monteroni, I-73100 Lecce, Italy.

<sup>4</sup> Max-Planck-Institut für Physik (Werner-Heisenberg-Institut), Föhringer Ring 6,  
D-80805 Munich, Germany.

**Abstract.** We perform a study of the ultra high energy neutrino detection performances of a  $\text{km}^3$  Neutrino Telescope sitting at the three proposed sites for **ANTARES**, **NEMO** and **NESTOR** in the Mediterranean sea. We focus on the effect of the underwater surface profile on the total amount of yearly expected  $\tau$  and  $\mu$  crossing the fiducial volume in the limit of full detection efficiency and energy resolution. We also emphasize the possible enhancement of matter effect by a suitable choice of the geometry of the Telescope.

PACS numbers: 95.85.Ry, 95.55.Vj, 13.15.+g

## 1. Introduction

Neutrinos are one of the main components of the cosmic radiation in the ultra-high energy (UHE) regime. Although their fluxes are uncertain and depend on the production mechanism, their detection can provide information on the sources and origin of the UHE cosmic rays. UHE neutrinos can be produced e.g. via  $\pi$ -photoproduction by strongly accelerated hadrons in presence of a background electromagnetic field. This scenario is expected to occur in extreme astrophysical environments like the cores of active galactic nuclei, radio galaxies and gamma ray burst sources as well as in the propagation of UHE nucleons scattering off the cosmic background radiation (known as *cosmogenic neutrinos* [1, 2]).

From the experimental point of view, neutrino astronomy in the UHE regime [3, 4, 5, 6, 7] is a rapidly developing field after the first pioneering and successful achievements, with a new generation of neutrino telescopes on the way. A benchmark result has been obtained by the **DUMAND** [8] collaboration, followed by the successful deployments of **NT-200** at Lake Baikal [9] and **AMANDA** [10] at the South Pole, which have shown the feasibility of large optical Cherenkov neutrino telescopes (NT) in open media like sea- or lake-water and glacial ice. These experiments observed atmospheric neutrinos [11] and set bounds on their extraterrestrial flux [12, 13] which are much more constraining than the corresponding bounds obtained by underground neutrino detectors [14]. These interesting results and the perspective to perform astronomical studies using UHE neutrinos stimulated several proposals for neutrino telescopes in the deep water of the Mediterranean sea, namely **ANTARES** [15], **NESTOR** [16] and **NEMO** [17], which in the future could lead to the construction of a  $\text{km}^3$  telescope as pursued by the **KM3NeT** project [18, 19]. A related project is **IceCube**, a cubic-kilometer under-ice neutrino detector [20, 21, 22, 23] currently being deployed in a location near the geographic South Pole in Antarctica. **IceCube** applies and improves the successful technique of **AMANDA** to a larger volume.

Although NTs were originally thought as  $\nu_\mu$  detectors, their capability as  $\nu_\tau$  detectors has become a hot topic [24, 25, 26, 27], in view of the fact that flavor neutrino oscillations lead to nearly equal astrophysical fluxes for the three neutrino flavors. Despite the different behavior of the produced tau leptons with respect to muons in terms of energy loss and decay length, both  $\nu_\mu$  and  $\nu_\tau$  detection are sensitive to the matter distribution near the NT site. Thus, a computation of the event detection rate of a  $\text{km}^3$  telescope requires a careful analysis of the surroundings of the proposed site. The importance of the elevation profile of the Earth surface around the detector was already found of some relevance in Ref. [28], where some of the present authors calculated the aperture of the Pierre Auger Observatory [29, 30] for Earth-skimming UHE  $\nu_\tau$ 's. Indeed, air shower experiments can be used as a NT at energies  $\gtrsim 10^{18}$  eV, a topic recently reviewed in [31]. In particular, the possibility of detection of the  $\tau$  leptons produced by Earth-skimming UHE  $\nu_\tau$ 's has been analyzed in a series of papers [28], [32]-[42]. In Ref. [28] the use of a Digital Elevation Map (DEM) of the geographical area of

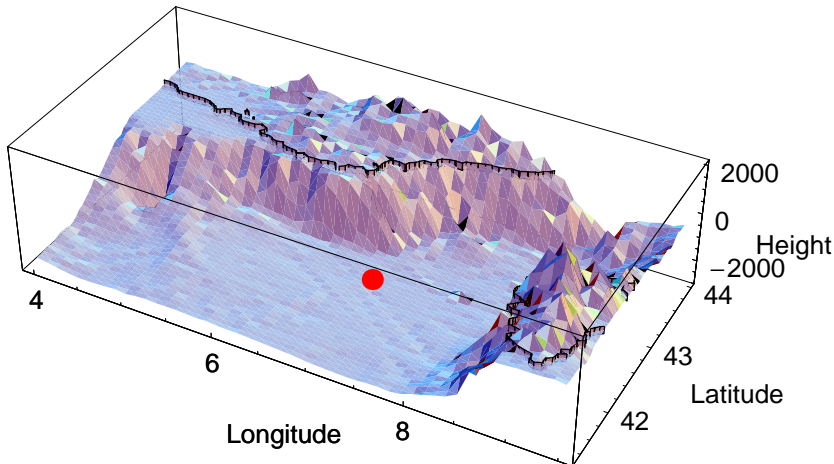


**Figure 1.** The surface profile of the area near the ANTARES site (red spot) at  $42^{\circ} 30$  N,  $07^{\circ} 00$  E. The black curve represents the coast line. The sea plateau depth in the simulation is assumed to be 2685 m.

the experiment proved useful to characterize peculiar matter effects in Earth-skimming events.

The aim of this paper is to estimate the effective aperture for  $\nu_\tau$  and  $\nu_\mu$  detection of a  $\text{km}^3$  NT in the Mediterranean sea placed at any of the three locations proposed by the ANTARES, NEMO and NESTOR collaborations. We do not consider any detail related to the experimental setup nor the detector response. In particular, we assume full detection efficiency via Cherenkov radiation for muons and tau's crossing the NT fiducial volume. We rather compare the site characteristics by using the DEM of the different areas. We shall therefore characterize and quantify the importance of “matter effects” for the three sites, and focus on the role played by the geometry of the experiment in enhancing the effect. These considerations may provide an important ingredient in shaping the final design of a  $\text{km}^3$  Mediterranean NT.

A detailed DEM of the under-water Earth surface is available from the Global Relief Data survey (ETOPO2) [43], a grid of altimetry measurements with a vertical resolution of 1 m averaged over cells of 2 minutes of latitude and longitude. In Figures 1, 2 and 3 we show the 3D maps of the areas around the three NT sites. The black curve represents the coast line, whereas the red spot stands for the location of the apparatus. By following the same approach developed in [28], we use this DEM to produce a realistic and statistically significant sample of  $\nu_\tau/\tau$  ( $\nu_\mu/\mu$ ) tracks crossing the fiducial volume of the NT that are then used to evaluate the effective aperture of each detector. We note that when the events are reconstructed only in terms of the energy loss along the track, the UHE tau's can not be distinguished from less energetic muons. This implies that the reconstruction analyses of  $\nu_\mu$  and  $\nu_\tau$  events are highly entangled issues. We shall consider both of them, although for the sake of clarity we will first

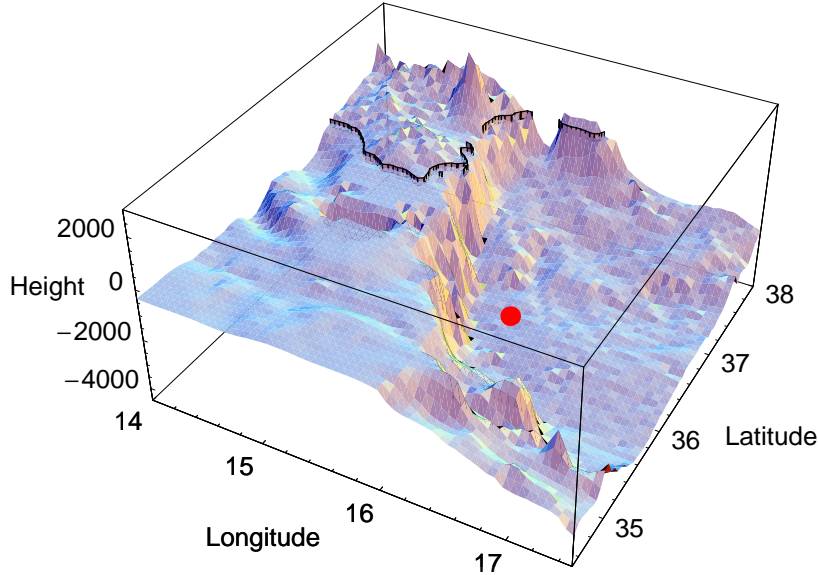


**Figure 2.** The surface profile of the area near the NEMO site (red spot) at  $36^{\circ} 21$  N,  $16^{\circ} 10$  E. The black curve represents the coast line. The sea plateau depth used in the simulation is 3424 m.

focus on  $\nu_\tau$  detection. We do not consider  $\tau$  regeneration effects which are expected to give a negligible contribution at PeV-EeV energies [44].

The structure of the paper is as follows. In Section 2 we introduce the formalism and definitions used in the analysis and define the aperture for a NT. Our results for  $\nu_\tau$  induced events are reported and discussed in Section 3 for various incoming neutrino fluxes, while  $\nu_\mu/\mu$  events are described in Section 4. Finally, we report our conclusions in Section 5.

## 2. The effective aperture of a NT

We define the  $\text{km}^3$  NT *fiducial* volume as that bounded by the six lateral surfaces  $\Sigma_a$  (the subindex  $a=W, E, N, S, U$  and  $D$  labels each surface through its orientation: West, East, North, South, Up, and Down), and indicate with  $\Omega_a \equiv (\theta_a, \phi_a)$  the generic direction of a track entering the surface  $\Sigma_a$ . The scheme of the NT fiducial volume and two examples of incoming tracks are shown in Fig. 4. We introduce all relevant quantities with reference to  $\nu_\tau$  events, the case of  $\nu_\mu$  being completely analogous.

Let  $d\Phi_\nu/(dE_\nu d\Omega_a)$  be the differential flux of UHE  $\nu_\tau + \bar{\nu}_\tau$ . The number per unit time of  $\tau$  leptons emerging from the Earth surface and entering the NT through  $\Sigma_a$  with

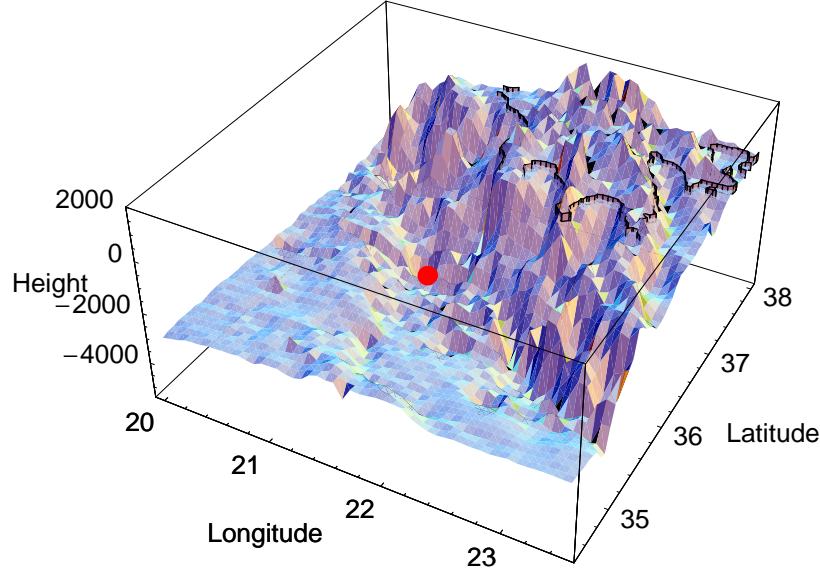


**Figure 3.** The surface profile of the area near the NESTOR site (red spot) at  $36^\circ 21$  N,  $21^\circ 21$  E. The black curve represents the coast line. The sea plateau depth in the simulation is assumed to be 4166 m.

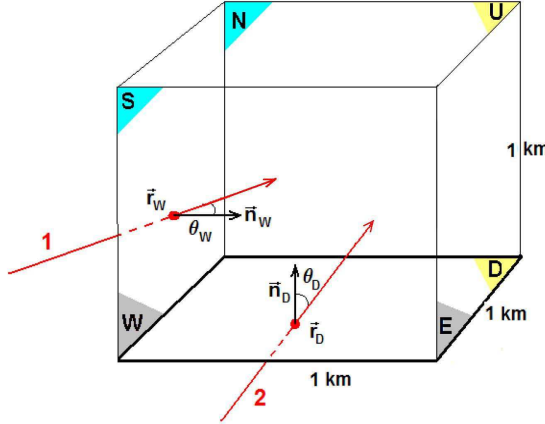


**Figure 4.** The angle definition and the fiducial volume of a  $\text{km}^3$  NT.

energy  $E_\tau$  is given by

$$\left( \frac{dN_\tau}{dt} \right)_a = \int d\Omega_a \int dS_a \int dE_\nu \frac{d\Phi_\nu(E_\nu, \Omega_a)}{dE_\nu d\Omega_a} \times \int dE_\tau \cos(\theta_a) k_a^\tau(E_\nu, E_\tau; \vec{r}_a, \Omega_a) . \quad (1)$$

This equation is the same as that in [28], but for full duty cycle and detection efficiency.

The kernel  $k_a^\tau(E_\nu, E_\tau; \vec{r}_a, \Omega_a)$  is the probability that an incoming  $\nu_\tau$  crossing the Earth, with energy  $E_\nu$  and direction  $\Omega_a$ , produces a  $\tau$ -lepton which enters the NT fiducial volume through the lateral surface  $dS_a$  at the position  $\vec{r}_a$  with energy  $E_\tau$  (see Fig. 4 for the angle definition). If we split the possible events between those with track intersecting the *rock* and the ones only crossing *water*, the kernel  $k_a^\tau(E_\nu, E_\tau; \vec{r}_a, \Omega_a)$  is given by the sum of these two mutually exclusive contributions,

$$k_a^\tau(E_\nu, E_\tau; \vec{r}_a, \Omega_a) = k_a^{\tau,r}(E_\nu, E_\tau; \vec{r}_a, \Omega_a) + k_a^{\tau,w}(E_\nu, E_\tau; \vec{r}_a, \Omega_a) . \quad (2)$$

Let us focus on the *rock* events contributing to  $k_a^{\tau,r}(E_\nu, E_\tau; \vec{r}_a, \Omega_a)$ . These can be classified according to their production mechanism as follows:

- 1) events in which the  $\nu_\tau$  interacts producing a  $\tau$  in the rock (r1);
- 2) events in which the  $\nu_\tau$  interacts producing a  $\tau$  in water, on the way to the NT (r2);
- 3) events in which the  $\nu_\tau$  interacts producing a  $\tau$  inside the NT fiducial volume (r3).

Therefore one has

$$k_a^{\tau,r}(E_\nu, E_\tau; \vec{r}_a, \Omega_a) = k_a^{\tau,r1}(E_\nu, E_\tau; \vec{r}_a, \Omega_a) + k_a^{\tau,r2}(E_\nu, E_\tau; \vec{r}_a, \Omega_a) + k_a^{\tau,r3}(E_\nu, E_\tau; \vec{r}_a, \Omega_a) . \quad (3)$$

Although here, for the sake of brevity, we only discuss in details the events occurring in rock (r1), the analysis of those of type (r2) and (r3) is completely analogous and straightforward and of course all contributions (r1)-(r3) have been added to compute the event rate.

As already shown in details in [28, 40] a (r1)-event corresponds to the simultaneous fulfillment of the following conditions:

- 1) A  $\nu_\tau$  with energy  $E_\nu$  travels over a distance  $z$  through the Earth before interacting.

The corresponding probability  $P_1$  is given by

$$P_1 = \exp \left\{ -\frac{z}{\lambda_{CC}^\nu(E_\nu)} \right\} , \quad (4)$$

where

$$\lambda_{CC}^\nu(E_\nu) = \frac{1}{\sigma_{CC}^{\nu N}(E_\nu) \varrho_r N_A} , \quad (5)$$

where  $\varrho_r \simeq 2.65 \text{ g/cm}^3$  is the average value of the rock density and  $N_A$  the Avogadro number. See [28, 40] for notations as well as a detailed discussion of the neutrino-nucleon cross section,  $\sigma_{CC}^{\nu N}(E_\nu)$ .

- 2) The neutrino produces a  $\tau$  in the interval  $z, z + dz$ , the probability of such an event being

$$P_2 dz = \frac{dz}{\lambda_{CC}^\nu(E_\nu)} . \quad (6)$$

We do not consider here the event corresponding to the scattering of a  $\nu_\tau$  via neutral current in the Earth followed by conversion via charged current, which amounts to a distortion of the incoming neutrino flux, the latter being yet unknown. Of course, this contribution should be added when trying to reconstruct the flux from experimental data.

3) The produced  $\tau$  emerges from the Earth rock with an energy  $E'_\tau$ . This happens with a probability

$$P_3 = \exp \left\{ -\frac{m_\tau}{c\tau_\tau \beta_\tau \varrho_r} \left( \frac{1}{E'_\tau} - \frac{1}{E_\tau^0(E_\nu)} \right) \right\} \times \delta \left( E'_\tau - E_\tau^0(E_\nu) e^{-\beta_\tau \varrho_r(z_r - z)} \right) , \quad (7)$$

where  $m_\tau = 1.78$  GeV,  $\tau_\tau \simeq 3.4 \times 10^{-13}$  s is the  $\tau$  mean lifetime and  $E_\tau^0$  the  $\tau$  energy at production, whereas the parameter  $\beta_\tau = 0.71 \times 10^{-6}$  cm<sup>2</sup> g<sup>-1</sup> weights the leading term in the  $\tau$  differential energy loss in rock [40, 45],

$$\frac{dE_\tau}{dz} = -(\beta_\tau + \gamma_\tau E_\tau) E_\tau \varrho_r . \quad (8)$$

The contribution of  $\gamma_\tau$  can be neglected as it only affects extremely energetic  $\tau$ 's which, differently from the case of the Pierre Auger Observatory, are not relevant for NTs. The quantity  $z_r(\vec{r}_a, \Omega_a)$  represents the total length in rock for a given track entering the lateral surface  $\Sigma_a$  of the fiducial volume at the point  $\vec{r}_a$  and with direction  $\Omega_a$ .

4) Finally, the  $\tau$  lepton emerging from the Earth rock propagates in water and enters the NT fiducial volume through the lateral surface  $\Sigma_a$  at the point  $\vec{r}_a$  with energy  $E_\tau$ . The corresponding survival probability is

$$P_4 = \exp \left\{ -\frac{m_\tau}{c\tau_\tau \beta_\tau \varrho_w} \left( \frac{1}{E_\tau} - \frac{1}{E'_\tau} \right) \right\} \delta \left( E_\tau - E'_\tau e^{-\beta_\tau \varrho_w z_w} \right) , \quad (9)$$

where  $\varrho_w$  stands for the water density and  $z_w(\vec{r}_a, \Omega_a)$  represents the total length in water before arriving to the fiducial volume for a given track entering the lateral surface  $\Sigma_a$  at the point  $\vec{r}_a$  and with direction  $\Omega_a$ .

Collecting together the different probabilities in Eqs. (4), (6), (7) and (9), we have

$$k_a^{\tau, r1}(E_\nu, E_\tau; \vec{r}_a, \Omega_a) = \int_0^{z_r} dz \int_0^{E_\tau^0(E_\nu)} dE'_\tau P_1 P_2 P_3 P_4 . \quad (10)$$

Similar results can be obtained for the (r2)- and (r3)-events as well as for those we defined as *water-like*.

For an isotropic flux we can rewrite Eq. (1), summing over all the surfaces, as

$$\begin{aligned} \frac{dN_\tau^{(r,w)}}{dt} &= \int dE_\nu \frac{1}{4\pi} \frac{d\Phi_\nu(E_\nu)}{dE_\nu} A^{\tau(r,w)}(E_\nu) \\ &= \sum_a \int dE_\nu \frac{1}{4\pi} \frac{d\Phi_\nu(E_\nu)}{dE_\nu} A_a^{\tau(r,w)}(E_\nu) , \end{aligned} \quad (11)$$

which defines the total aperture  $A^{\tau(r,w)}(E_\nu)$ , with "r" and "w" denoting the *rock* and *water* kind of events, respectively. The contribution of each surface to the total aperture reads

$$A_a^{\tau(r,w)}(E_\nu) = \int dE_\tau \int d\Omega_a \int dS_a \cos(\theta_a) k_a^{\tau, (r,w)}(E_\nu, E_\tau; \vec{r}_a, \Omega_a) . \quad (12)$$

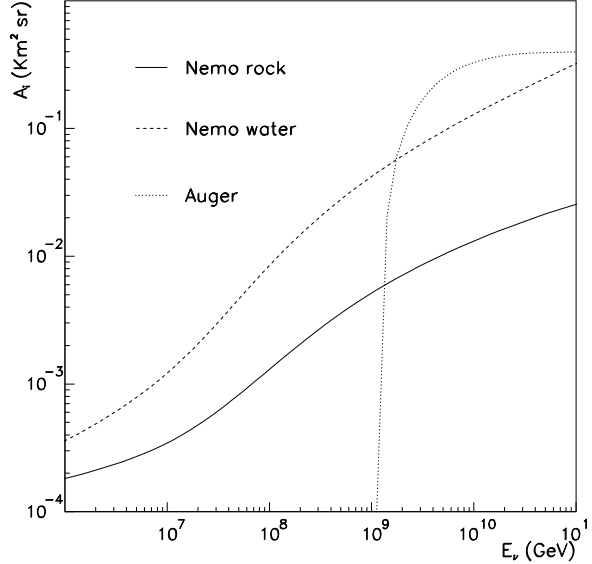


**Figure 5.** The effective apertures  $A^{\tau(r)}(E_\nu)$  (solid line) and  $A^{\tau(w)}(E_\nu)$  (dashed line) defined in Eq. (11) versus neutrino energy for NEMO. The dotted line corresponds to the same quantity for the Auger Fluorescence Detector for Earth-skimming  $\nu_\tau$  as in [28].

### 3. The event rate for $\nu_\tau$ interactions

We show in Fig. 5 the apertures  $A^{\tau(r,w)}$  for the NEMO site together with the corresponding quantity for the Pierre Auger Observatory Fluorescence Detector (FD) calculated in [28]. Note that the Auger case is only for Earth-skimming  $\tau$ 's, since down-going neutrino induced events can be disentangled from ordinary cosmic rays only for very inclined showers. Interestingly, the NEMO-water and Auger-FD apertures almost match at the FD threshold of  $10^{18}$  eV, so that using both detectors results into a wide energy range of sensitivity to  $\nu_\tau$  fluxes.

We show in Fig. 6 the high energy behavior for each surface contributing to the effective aperture. For *rock* events there is a clear W-E asymmetry, easily understood in terms of matter effects related to the particular morphology of the NEMO site (see Fig. 2). A much smaller S-N asymmetry is also present. For neutrino energies larger than  $10^7$  GeV the main contribution to the aperture  $A^{\tau(r)}(E_\nu)$  comes from the lateral surfaces, i.e. from  $\tau$  leptons emerging from the rock far from the NT basis and crossing the fiducial volume almost horizontally. Instead, the upper surface contribution is negligible due to the very small fraction of events crossing the rock and entering the detector from above. For *water* events the contribution to the aperture from all surfaces is comparable (except for the lower one which has no events), the upper one providing a slightly larger contribution as the energy decreases. Indeed, events which would cross the lateral surfaces should travel over a longer path in water and this becomes more unlikely at lower energies due to the shorter  $\tau$  decay length.

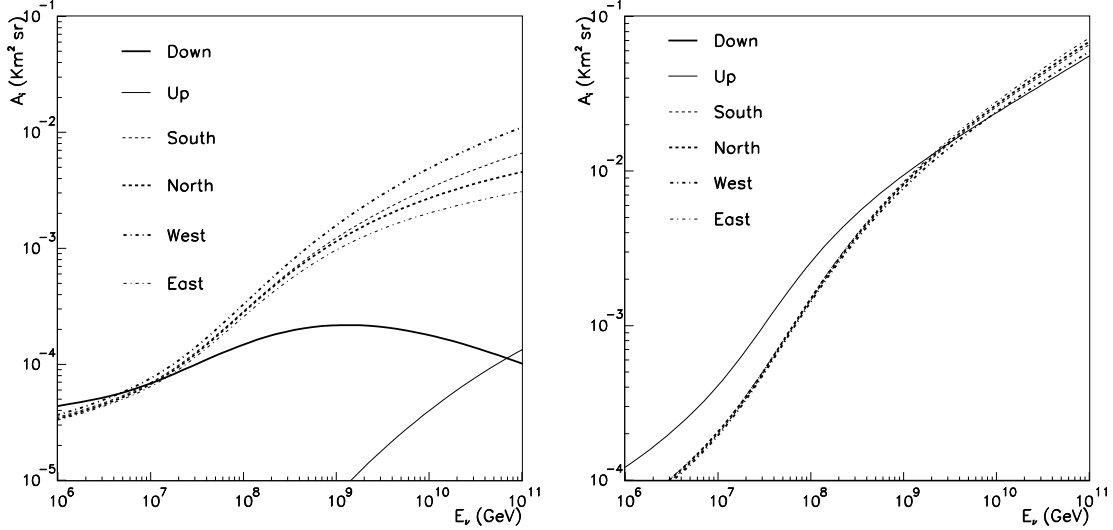


**Figure 6.** The effective apertures  $A_a^{\tau(r,w)}(E_\nu)$  of Eq. (12) versus neutrino energy for (left) *rock* events and (right) *water* events for the NEMO site.

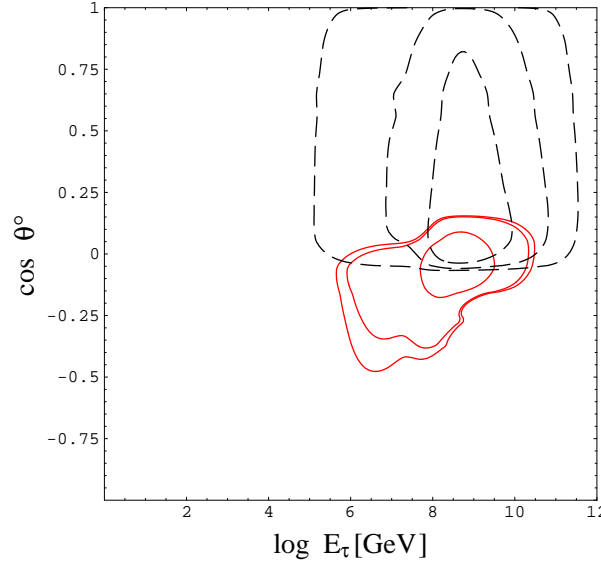


**Figure 7.** Contour plot in the plane zenith angle- $\tau$  energy for the NEMO site and for *rock* (red full lines) and *water* (black dashed lines) events. In both cases the contours enclose 68, 95 and 99 % of the total number of events calculated assuming a GZK-WB flux.  $\cos \theta = 1, 0, -1$  correspond respectively to down-going, earth-skimming, and up-going events.

In Fig. 7 we report, for both the *rock* and *water* cases and for the NEMO site, the contours enclosing 68, 95 and 99 % of the total event rate, as they appear in the plane  $E_\tau$ -arrival zenith  $\theta$ . These results were obtained assuming a Waxmann-Bahcall-like neutrino flux (GZK-WB) [46] (see also [28] and references therein). As the energy increases, the

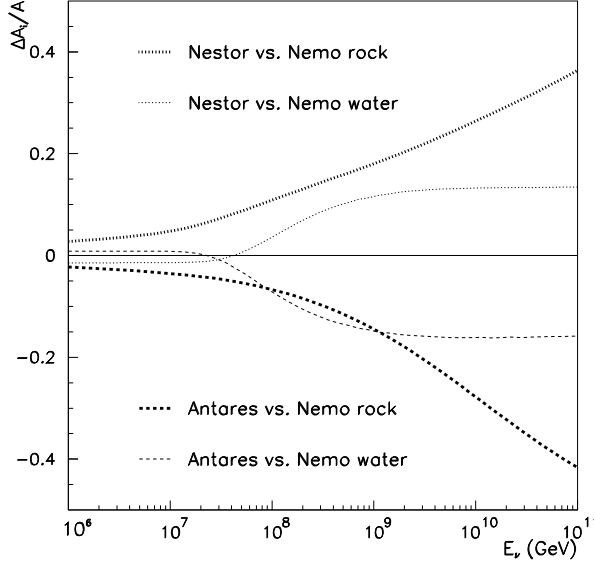


**Figure 8.** A comparison of the effective apertures  $A^{\tau((r,w))}(E_\nu)$  for the three NT sites. We plot the ratios  $[A^{\tau((r,w))}(\text{NESTOR}) - A^{\tau((r,w))}(\text{NEMO})]/A^{\tau((r,w))}(\text{NEMO})$  and  $[A^{\tau((r,w))}(\text{ANTARES}) - A^{\tau((r,w))}(\text{NEMO})]/A^{\tau((r,w))}(\text{NEMO})$  versus the neutrino energy.

arrival directions of *rock* events are almost restricted to the horizontal (Earth-skimming), while at lower energies the earth-screening effect is less pronounced and this explains the broader angular distribution. The situation is different for *water* events for which the angular distribution is broad at all energies, a purely geometrical effect due to the fact that (down-going) *water* events are not screened in few kilometers of water. The same geometrical considerations explain the ratio of *water* to *rock* event rate of  $\mathcal{O}(10)$  (see below) which is simply related to the ratio of down-going to Earth-skimming solid angles. This is the same kind of behavior expected in the Auger detector although, as we already mentioned, the down-going events in this case are indistinguishable from the background of proton-induced showers so that only Earth-skimming or almost horizontal showers can be used to identify unambiguously the neutrino-induced events. It is also worth noticing the expected  $\tau$  energy distribution shown in Fig. 7. All events correspond to a relatively narrow window, from  $10^6$  GeV up to  $10^{10}$  GeV, where the lower cut-off arises from the shorter  $\tau$  decay length at low energy.

In Fig. 8 we compare the detection performances of a  $\text{km}^3$  NT placed at one of the three sites in the Mediterranean sea. The NESTOR site shows the highest values of the  $\tau$ -aperture for both *rock* and *water*, due to its larger depth and the particular matter distribution of the surrounding area, while the lowest rates are obtained for ANTARES. The aperture in the three sites can be quite different at high energy but the net effect of this on the expected number of events per year is not particularly significant since the UHE neutrino flux drops rapidly with the energy.

Knowing the aperture of the NT at each site, we can compute the expected  $\tau$  event

Surf.	ANTARES	NEMO	NESTOR
D	0.0086/0	0.0086/0	0.0085/0
U	0/0.1741	0.0002/0.2191	0.0003/0.2595
S	0.0219/0.1635	0.0290/0.1799	0.0287/0.2014
N	0.0275/0.1573	0.0268/0.1847	0.0359/0.1938
W	0.0247/0.1616	0.0371/0.1715	0.0303/0.2020
E	0.0240/0.1622	0.0228/0.1900	0.0414/0.1858
Total	0.107/0.819	0.124/0.945	0.145/1.043

**Table 1.** Estimated rate per year of *rock/water*  $\tau$  events at the three  $\text{km}^3$  NT sites for a GZK-WB flux. The contribution of each detector surface to the total number of events is also reported.

rate, once a neutrino flux is specified. In Table 1 these rates are shown assuming a GZK-WB flux. The enhancement effect due to the local matter distribution is responsible for the N-S, W-E and NE-SW asymmetries for the **ANTARES**, **NEMO** and **NESTOR** sites, respectively, as expected from the matter profiles shown in Figs. 1, 2 and 3. These matter effects, for the specific UHE flux considered (GZK-WB), correspond to an enhancement of *rock* events of the order of 20% and a screening factor for *water* events of the order of a few percent. This is easily understood since for *water* events the U surface gives a significant contribution which is essentially unaffected by matter distribution.

It is important to emphasize that the role of matter effects depends critically upon the energy spectrum of the UHE neutrino flux. For more energetic neutrino fluxes the enhancement factor is expected to be more significant (see the energy behavior of  $A_a^{\tau(r)}(E_\nu)$  in Fig. 6).

In Table 2 the rate of *rock/water*  $\tau$  events are computed for the three different  $\text{km}^3$  NT sites using several UHE neutrino fluxes as already considered in [28, 40] and described in [46]-[52] (see also Fig. 11). For comparison, we also show in the last column the corresponding prediction for Earth-skimming  $\nu_\tau$  at Auger-FD. As can be seen from Table 2, the enhancement factors due to matter effects on *rock* events can be as large as 30%, whereas the difference in the rates of *water* events for a fixed neutrino flux is mainly due to the different depth of the three sites.

An interesting feature is the dependence of the event rate upon the shape of the NT detector for a fixed total volume of  $1 \text{ km}^3$  a property that might be relevant for the eventual design of the detector. Consider for example a  $\text{km}^3$  NT placed at the **NEMO** site with the shape of a parallelepiped rather than a cube, where in particular the E and W surfaces are enlarged by a factor 3 in the horizontal dimension, the N and S surfaces being reduced by the same factor, keeping the height of towers still of 1 km. In this case the expected rate of *rock* events per year is enhanced by almost a factor 2, from 0.12 to 0.21 for the GZK-WB flux, while this enhancement could be even larger for neutrino fluxes with a larger high energy component. Moreover, the expected rate of *water* events increases as well by a factor of the order of 50%, from 0.945 up to

$\nu$ -fluxes	ANTARES	NEMO	NESTOR	Auger-FD [28]
GZK-WB	0.107/0.819	0.124/0.945	0.145/1.043	0.074
GZK-L	0.110/1.106	0.141/1.308	0.175/1.471	0.213
GZK-H	0.245/2.284	0.335/3.348	0.423/3.777	0.560
NH	1.029/8.920	1.248/10.37	1.488/11.51	1.245
TD	0.837/5.181	0.957/5.888	1.087/6.436	0.548

**Table 2.** Yearly rate of *rock/water*  $\tau$  events at the three  $\text{km}^3$  NT sites for different UHE neutrino fluxes. GZK-H is for an initial proton flux  $\propto 1/E$ , assuming that the EGRET flux is entirely due to  $\pi$ - photoproduction. GZK-L shows the neutrino flux when the associated photons contribute only up to 20% in the EGRET flux. GZK-WB stands for an initial proton flux  $\propto 1/E^2$  [46]–[50]. The other two neutrino fluxes correspond to more exotic UHECR models. NH represents the neutrino flux prediction in a model with new hadrons [51], whereas TD is the neutrino flux for a topological defect model [52]. In the last column we report the corresponding prediction for Earth-skimming  $\nu_\tau$  at Auger-FD.

1.425 per year. Similar exercises can be also performed for the ANTARES and NESTOR sites. Of course, a further possibility which might favor UHE- $\tau$  detection consists in increasing the effective volume of the detector keeping unchanged the 1 km height and the number of towers of photomultipliers but adopting a larger spacing. As an example, for a factor four larger volume with a doubling of the tower spacing both the *rock* and *water*  $\tau$  events would increase by almost a factor two, but obviously at the expense of the energy threshold and the quality of the event reconstruction for “low-energy” (TeV) neutrinos. For a detector aiming at the exploration of the range above the PeV, this is a less severe problem.

The fact that the event rate depends upon the total surface of the detector is a peculiar feature of a NT, quite differently from what expected at the Auger observatory. Actually, in this case observed showers are generally initiated not very far from the detector compared to its dimensions so that the shape of the detector is not as important as its volume. In fact, in order to produce a  $\tau$  emerging from the Earth with enough energy to generate a shower detectable by the Auger FD (at least 1 EeV =  $10^{18}$  eV), the energy of the neutrino should be larger than  $10^{18}$  eV, taking into account the  $\tau$  energy loss in the rock. But the decay length of such a UHE  $\tau$  is  $l_{\text{decay}} \simeq 50 \text{ km} \times (E_\tau/\text{EeV})$ , to be compared with the dimensions of the Auger fiducial volume,  $\sim 50 \times 60 \times 10 \text{ km}^3$ . Conversely, a neutrino telescope can detect tau’s or muons which are produced very far from the detector by a neutrino charged-current interaction, from distances comparable to the charged lepton range at that particular energy [27]. Indeed, the  $\tau$  range in water is of the order of several kilometers: from the value of  $\beta_\tau = 0.71 \times 10^{-6} \text{ cm}^2 \text{ g}^{-1}$  we obtain an attenuation length  $1/(\beta_\tau \varrho_w) \simeq 15 \text{ km}$ , while for muons (see next section) the range is approximately eight times smaller, of the order of 2 km. In other words, the effective volume of a NT of the kind discussed so far can be much larger than  $1 \text{ km}^3$ , thus maximizing the detector area might greatly improve the detection rate.

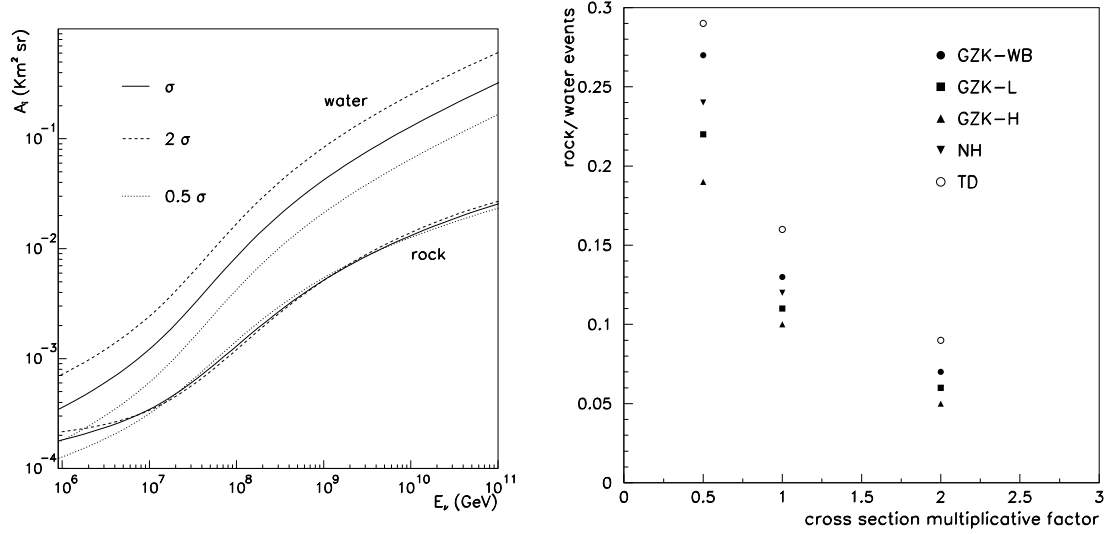


**Figure 9.** (Left) The effective apertures  $A^{\tau(r,w)}(E_\nu)$  for the NEMO site for a  $\nu_\tau$ -nucleon cross section multiplied by a factor 0.5, 1 and 2 with respect to the standard result  $\sigma$ . (Right) Ratios of the number of events in *rock/water* when the cross section is rescaled by the factor shown on the *x* axis, for several incoming UHE neutrino fluxes.

Of course, we should not forget that the design of a NT also depends strongly upon more detailed experimental considerations. Shapes which are not very compact or a detector with very sparse instrumentation have worse performances in the reconstruction of track properties as well as in signal-background separation, though this is mainly problematic at energies lower than 100 TeV, in the atmospheric neutrino energy range. In any case, our analysis suggests that the choice of the detector shape could be an important feature in orienting the target of a NT investigation towards either atmospheric or extra-atmospheric neutrino physics. In this respect, the possibility to modify this parameter quite easily for a NT water detector offers a great advantage with respect to an under-ice detector.

One of the main motivations for studying UHE neutrinos is that they provide a possibility to explore a range of energies for scattering processes which is still untested (maybe impossible to test) by particle accelerators. In this respect, measuring the neutrino–nucleon cross sections at high energies could have a large impact on constraining or discovering new physics beyond the standard model (see e.g. [26, 53]). While a measurement of the event energy spectrum cannot remove in general a degeneracy between the neutrino cross section and the incoming neutrino flux, a neutrino telescope could offer the interesting capability of disentangling these two factors because of the role of matter effects. Indeed, provided that enough statistics is collected and the detector has a good zenith angle resolution, the flux dependence can be subtracted off by measuring the ratio of the event rates coming from different directions [54, 55, 56]. In the left panel of Fig. 9 we show how the NEMO effective apertures for  $\tau$  *rock* and *water* events change if the neutrino-nucleon cross section is half or twice the standard model

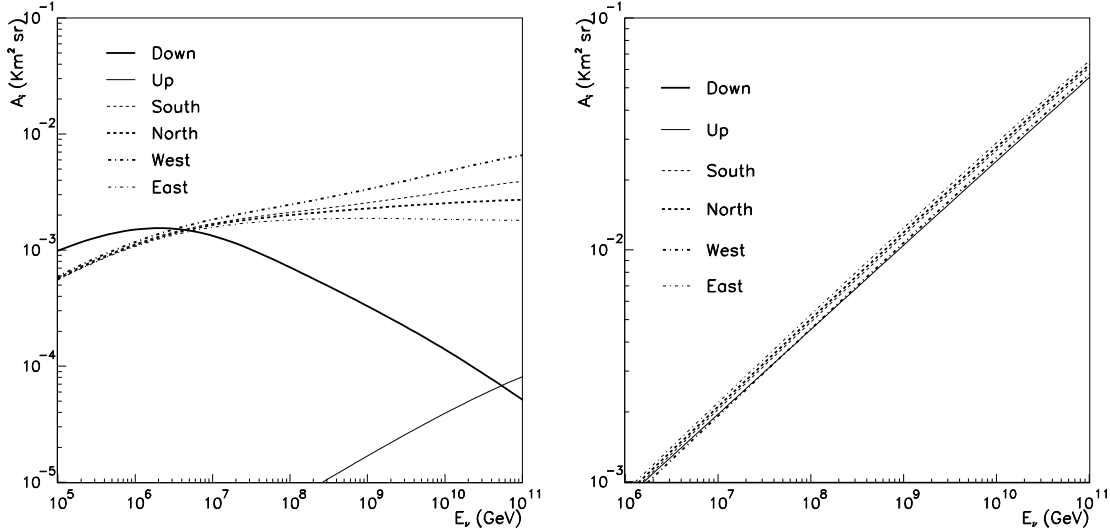


**Figure 10.** The effective apertures  $A_a^{\mu(r,w)}(E_\nu)$  versus the neutrino energy for (left) *rock* events and (right) *water* events at the NEMO site.

result while in the right panel we display the ratio of *water/rock*  $\tau$  event rates for several adopted fluxes. We see that this ratio is quite sensitive to the value of the cross section. In particular, the number of *rock* events is essentially unaffected while the *water* event rate increases almost linearly with the cross section. Clearly, since the statistical error on the ratio would be dominated by the rare *rock* events, an experiment which aims at exploiting this effect should maximize the acceptance for almost horizontal events. We conclude by noticing that our results do not take into account any detailed experimental setup and up to this point the  $\nu_\mu$  contribution is not yet considered. Nevertheless, since both the incoming neutrino flux and cross section on nucleons are expected to be flavor independent the possibility of determining both these quantities at a NT seems an interesting perspective. A more detailed analysis of this issue will be addressed elsewhere.

#### 4. The $\nu_\mu$ contribution: disentangling muons from $\tau$ 's

In the previous Section we have discussed the rate of  $\nu_\tau$  events implicitly assuming that a  $\tau$  lepton can be distinguished from a muon in a NT. However, given the experimental characteristics of the detector, this could be a difficult task and  $\nu_\mu$  events should be also included in any realistic simulation. We address this issue in the present Section.

Using the definition of the aperture in full analogy with Eq. (12) and applying the same considerations of Section 2 to  $\nu_\mu/\mu$ , we have computed the  $\mu$  apertures for *water* and *rock* events for the various surfaces of the NT, adopting the value  $\beta_\mu = 0.58 \times 10^{-5}$   $\text{cm}^2 \text{ g}^{-1}$  in the expression of the muon differential energy loss analogous to Eq. (8) (as for the  $\tau$ , the term weighted by  $\gamma_\mu$  is negligible for the energy range of interest). The results are shown in Fig. 10. The main features as well as the role of matter effects are

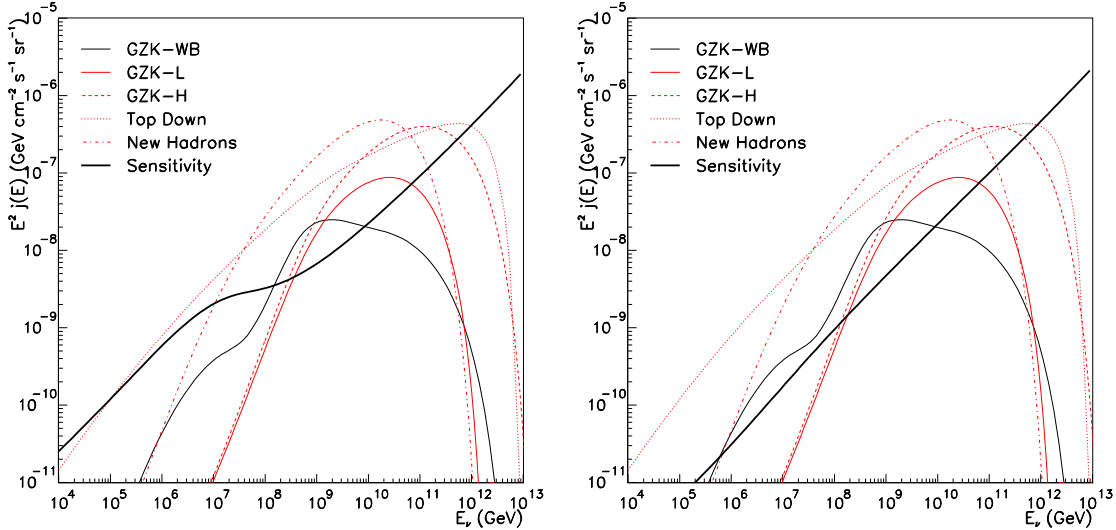


**Figure 11.** The total NEMO sensitivities for (left)  $\tau$  and (right)  $\mu$  events versus the neutrino energy, compared with the UHE neutrino fluxes considered in the paper.

essentially unchanged for muons, the only difference coming from the muon contribution at lower energies because of the longer muon lifetime compared to that of tau's.

It is worthwhile briefly discussing the adopted parametrization for muon and tau energy losses. At energies larger than  $10^6$  GeV, tau energy losses are affected by the large theoretical uncertainty on cross-section for photonuclear interaction, the leading mechanism at these energies (see [40] and [57], and references therein). We use the simple parametrization of Eq. (8), which is accurate enough given this intrinsic theoretical uncertainty.

On the other hand, photonuclear interactions are less relevant for muon propagation, thus the theoretical uncertainty on the energy loss is correspondingly smaller. We then checked the validity of the approximation given in Section 4 versus the detailed calculation given in [58]. We found that the accuracy is at the level of 15% over the whole energy range. The impact of this uncertainty on the expected event rate is as follows: a 15% increase of  $\beta_\mu$  gives a few % decrease of the number of water events and an  $\sim 10$  % decrease of the number of rock events. This uncertainty then doesn't affect the estimate of the number of  $\nu_\mu$  events while, likely, a more careful treatment is required for a reliable forecast of the neutrino cross-section sensitivities at a Neutrino Telescope.

In Fig. 11 we summarize the  $\tau$  and  $\mu$  results by showing the total sensitivity  $S^{\mu,\tau}$  for NEMO defined as  $S^{\mu,\tau} E_\nu A^{\mu,\tau} = 1$  event year $^{-1}$  ( $E_\nu$  decade) $^{-1}$ , with  $A^{\mu,\tau}$  the total  $\mu$  and  $\tau$  effective aperture, respectively. We also show in the same plot the various neutrino fluxes considered through the paper. We see that in agreement with the results of Table 2, at least one event per year is expected even in the pessimistic case of a GZK-WB flux, while larger rates are expected for higher fluxes (see also [59]). Notice that in the energy bin  $10^8$ - $10^{10}$  GeV both  $\mu$  and  $\tau$  contributions are comparable while muons are

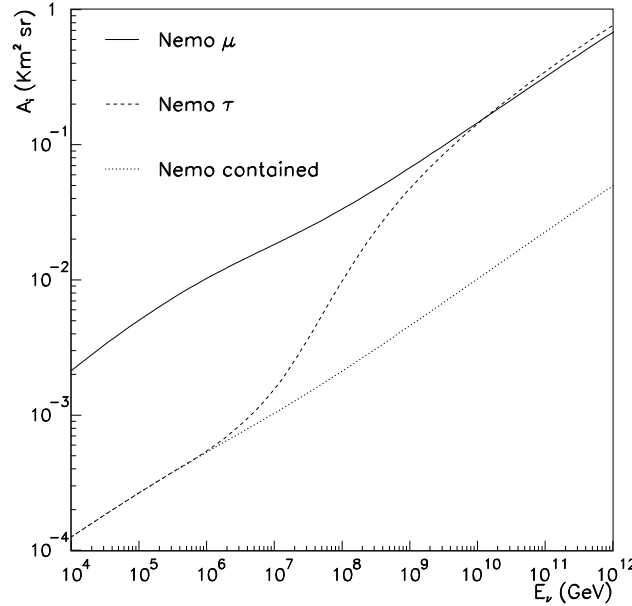


**Figure 12.** Total  $\tau$ ,  $\mu$  and contained events apertures for the NEMO site.

expected to dominate in the lower energy range, depending on the particular flux we consider.

What are the real possibilities of disentangling  $\tau$  and muons? As we mentioned in the Introduction, the main difficulty is that Cherenkov detectors like a NT do not measure the particle energy but rather the energy loss inside the detector volume and thus a high-energy  $\tau$  can be misidentified with a muon of lower energy. This is because the ratio of  $\tau$  to  $\mu$  energy loss rate is given by  $\beta_\tau/\beta_\mu \approx 1/8$ . An efficient identification is expected for contained events, since in this case an extra piece of information is available from the neutrino interaction vertex and this is typically sufficient to distinguish a muon from a  $\tau$  production event as confirmed by recent Monte Carlo simulations [60]. We show in Fig. 12 the total apertures for  $\tau$  and  $\mu$  events at the NEMO site together with the aperture for contained events. Indeed, contained events represent a relevant fraction of the total number of events, always of the order of 10% for  $\mu$  and even greater for low energy  $\tau$  ( $\lesssim 10^7$  GeV=10 PeV) due to the very short ( $\lesssim 1$  km) decay length at these energies. Moreover, the contained aperture depends only on the neutrino interaction probability so that it can be considered also a reliable estimate of the  $e$ -induced showering events, neglecting the (small) effect of the Glashow  $\bar{\nu}_e e^-$  resonance at 6.3 PeV. It may also be possible to identify *lollipop* events in which a  $\nu_\tau$  with energy larger than PeV produces a long minimum-ionizing track that enters the detector and eventually ends in a huge burst as the  $\tau$  lepton decays into a final state with hadrons or an electron. In this case, the final burst would be a direct measurement of the  $\tau$  energy while the energy loss along the track would be smaller than for a muon of the same energy. Perhaps, the cleanest signature of a  $\tau$  particle would be the detections of a double-bang event [61] in which a  $\nu_\tau$  interacts inside the detector and the produced  $\tau$

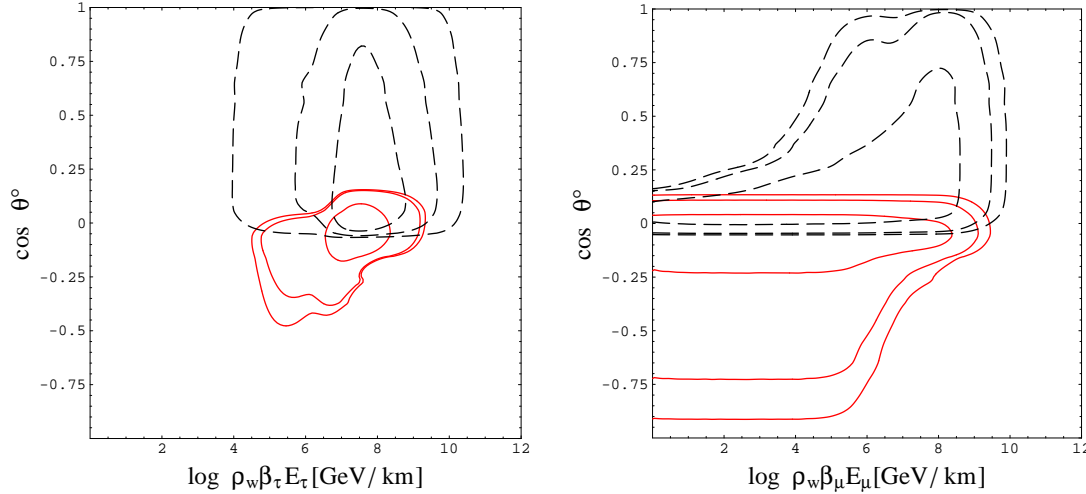


**Figure 13.** Contour plots of the number of *rock* events (red full lines) and *water* events (black dashed lines) at the NEMO site in the zenith angle-dE/dx plane for  $\tau$  (left panel) and  $\mu$  (right panel) assuming a GZK-WB neutrino flux. The contours enclose 65, 95 and 99 % of the total number of events.

decays in shower again in the detector, but the probability of such an event is extremely small. In any case, all these possibilities suffer from a very low statistics as they all require that the interactions (showering or production) occur inside the detector, with a reduction of the effective volume down to  $1 \text{ km}^3$  compared with the several  $\text{km}^3$  effective volume for  $\mu$  and  $\tau$  events which go across the NT fiducial volume.

In view of these considerations, we conclude that the most viable strategy is to combine both muon and tau contributions and construct spectra depending upon quantities which are directly observable. The simplest choice is to consider the energy loss rate inside the detector which amounts to measure the track length and the total deposited energy and the arrival direction. In Fig. 13 we show the contours of expected  $\mu$  and  $\tau$  events in terms of the zenith angle of arrival directions and  $dE/dx \simeq -\beta E \rho_w$ . We see that for low energy losses the whole contribution comes from muons which therefore, can be easily disentangled, whereas in the high energy loss tails the event distributions are almost the same for both neutrino flavors and one is forced to use the total  $\nu_\mu + \nu_\tau$  events as the input of any analysis of the data.

## 5. Conclusions

The UHE neutrinos represent one of the main issues for several experiments which adopt a variety of detection techniques. Among these, the optical Cherenkov neutrino telescopes, deployed under water or ice, look for the charged leptons produced by the UHE neutrinos that reach the Earth. In this paper, we have presented a new study of the performance of a  $\text{km}^3$  neutrino telescope to be located in any of the three sites in the

Mediterranean sea proposed by the ANTARES, NEMO, and NESTOR collaborations. We have considered in details the under-water surface profile of each of the three sites, using the data from a Digital Elevation Map. By generating a realistic and statistically significant sample of  $\nu_\tau/\tau$  tracks crossing the fiducial volume of the  $\text{km}^3$  neutrino telescope, we have calculated its effective aperture to UHE  $\nu_\tau$  neutrinos and the expected number of events for different UHE neutrino fluxes, for both cases where the charged lepton is produced in rock and water near the telescope site.

Although we have not included detector-specific features, like partial detection efficiency and finite energy resolution, our results show that the impact of the site geography (or matter effects) on observables such as the total number of events or asymmetries in the event direction can be important.

These matter effects can be enhanced by a suitable choice of the geometry of the telescope with a fixed volume. We have also discussed the possibility of obtaining information on both the neutrino flux and the neutrino-nucleon cross section in the UHE range by measuring the ratio of rock and water events.

Finally, we have discussed the contribution of muon neutrinos to the event rate of the telescope. We found that the number of muon events is comparable to that of tau, depending on the considered energy range and UHE neutrino flux. We have briefly discussed the problem of whether it is possible to distinguish muons and  $\tau$ 's in the detector and stressed that a safe strategy is to consider the sum over the neutrino flavor events versus the two variables which can be directly measured in the apparatus, namely the arrival direction and the energy loss rate in the fiducial volume. Of course, since from neutrino oscillations we expect almost equal fluxes of  $\nu_\mu$  and  $\nu_\tau$  this not limits in any respect the possibility of using under water NT to perform neutrino astronomy and flux reconstruction.

## Acknowledgments

We are pleased to thank G. Barbarino, G. Longo and E. Migneco for useful comments and discussions. This work was supported by a Spanish-Italian AI, the Spanish grants FPA2005-01269 and GV/05/017 of Generalitat Valenciana, a MEC-INFN agreement as well as the PRIN04 "Fisica Astroparticellare" of Italian MIUR. SP was supported by a Ramón y Cajal contract of MEC. PS acknowledges the support by the Deutsche Forschungsgemeinschaft under grant SFB 375 and by the European Network of Theoretical Astroparticle Physics ILIAS/N6 under contract number RII3-CT-2004-506222.

## References

- [1] Berezinsky V S and Zatsepin G T, 1969 *Phys. Lett. B* **28** 423.
- [2] Berezinsky V S and Zatsepin G T, 1970 *Sov. J. Nucl. Phys.* **11** 111 (1970 *Yad. Fiz.* **11** 200).
- [3] Gaisser T K, Halzen F and Stanev T, 1995 *Phys. Rep.* **258** 173.
- [4] Learned J G and Mannheim K, 2000 *Ann. Rev. Nucl. Part. Sci.* **50** 679.
- [5] Spiering C, 2002 *Prog. Particle Nucl. Phys.* **48** 43.

- [6] Halzen F and Hooper D, 2002 *Rept. Prog. Phys.* **65** 1025.
- [7] McDonald A B et al., 2004 *Rev. Sci. Instrum.* **75** 293.
- [8] Grieder P K F et al., 1995 *Nucl. Phys. Proc. Suppl.* **43** 145.
- [9] Balkanov V A et al., 1999 *Nucl. Phys. Proc. Suppl.* **75A** 409.
- [10] Andres E et al., 2000 *Astropart. Phys.* **13** 1.
- [11] Ahrens J et al., 2002 *Phys. Rev. D* **66** 012005.
- [12] Belolaptikov I A et al., 2000 *Phys. Atom. Nucl.* **63** 951.
- [13] Ahrens J et al., 2003 *Phys. Rev. Lett.* **90** 251101.
- [14] Ambrosio M et al, 2003 *Astropart. Phys.* **19** 1.
- [15] Aslanides E et al., 1999 *A Deep Sea Telescope for High Energy Neutrinos, Proposal*, [astro-ph/9907432].
- [16] Bottai S, 1999 Contribution to 26th ICRC, Salt Lake City, AIP Conf. Proc. **516** vol 2 456.
- [17] Riccobene G, 2002 Proc. of the Workshop on Methodical Aspects of Underwater/Ice Neutrino Telescopes, 61
- [18] Katz U F, 2006 *Prog. Part. Nucl. Phys.* **57** 273.
- [19] Katz U F, 2006 [astro-ph/0606068].
- [20] Ahrens J et al., 2000 *The IceCube NSF Proposal*.
- [21] Biron A et al., 2001 *Participation of DESY-Zeuthen in the IceCube Project, Proposal to the DESY PRC*.
- [22] Ahrens J et al., 2001 *IceCube Conceptual Design Document*.
- [23] Ahrens J et al., 2004 *Astropart. Phys.* **20** 507.
- [24] Dutta S I, Reno M H and Sarcevic I, 2000 *Phys. Rev. D* **62** 123001.
- [25] González-García M C, Halzen F and Maltoni M, 2005 *Phys. Rev. D* **71** 093010.
- [26] Anchordoqui L and Halzen F, 2005 [hep-ph/0510389].
- [27] Yoshida S, Ishibashi R and Miyamoto H, 2004 *Phys. Rev. D* **69** 103004.
- [28] Miele G, Pastor S and Pisanti O, 2006 *Phys. Lett. B* **634** 137.
- [29] Pierre Auger Collaboration, 1996 *The Pierre Auger Project Design Report*, FERMILAB-PUB-96-024.
- [30] Abraham J et al. (Pierre Auger Collaboration), 2004 *Nucl. Instrum. Meth. A* **523** 50.
- [31] Zas E, 2005 *New J. Phys.* **7** 130.
- [32] Capelle K S, Cronin J W, Parente G and Zas E, 1998 *Astropart. Phys.* **8** 321.
- [33] Fargion D, Aiello A and Conversano R, 1999 Contribution to 26th ICRC, Salt Lake City, AIP Conf. Proc. **516** vol 2 396.
- [34] Becattini F and Bottai S, 2001 *Astropart. Phys.* **15** 323.
- [35] Fargion D, 2002 *Astrophys. J.* **570** 909.
- [36] Letessier-Selvon A, 2000 *AIP Conf. Proc.* **566** 157.
- [37] Bertou X et al., 2002 *Astropart. Phys.* **17** 183.
- [38] Feng J L, Fisher P, Wilczek F and Yu T M, 2002 *Phys. Rev. Lett.* **88** 161102.
- [39] Fargion D, De Sanctis Lucentini P G and De Santis M, 2004 *Astrophys. J.* **613** 1285.
- [40] Aramo C et al., 2005 *Astropart. Phys.* **23** 65.
- [41] Cao Z, Huang M A, Sokolsky P and Hu Y, 2005 *J. Phys. G* **31** 571.
- [42] Miele G, Perrone L and Pisanti O, 2005 *Nucl. Phys. Proc. Suppl.* **145** 347.
- [43] U.S. Department of Commerce, National Oceanic and Atmospheric Administration, National Geophysical Data Center, 2001 *2-minute Gridded Global Relief Data (ETOPO2)*, <http://www.ngdc.noaa.gov/mgg/fliers/01mgg04.html>
- [44] Halzen F and Saltzberg D, 1998 *Phys. Rev. Lett.* **81** 4305.
- [45] Dutta S I, Huang Y and Reno M H, 2005 *Phys. Rev. D* **72** 013005.
- [46] Waxman E and Bahcall J N, 1999 *Phys. Rev. D* **59** 023002.
- [47] Kalashev O E, Kuzmin V A and Semikoz D V, 1999 [astro-ph/9911035].
- [48] Kalashev O E, Kuzmin V A and Semikoz D V, 2001 *Mod. Phys. Lett. A* **16** 2505.
- [49] Kalashev O E, Kuzmin V A, Semikoz D V and Sigl G, 2002 *Phys. Rev. D* **66** 063004.

- [50] Semikoz D V and Sigl G, 2004 *JCAP* **0404** 003.
- [51] Kachelriess M, Semikoz D V and Tórtola M A, 2003 *Phys. Rev. D* **68** 043005.
- [52] Bhattacharjee P and Sigl G, 2000 *Phys. Rep.* **327** 109.
- [53] Anchordoqui L A et al., 2005 *Phys. Rev. D* **72** 065019.
- [54] Kusenko A and Weiler T J, 2002 *Phys. Rev. Lett.* **88** 161101.
- [55] Hooper D, 2002 *Phys. Rev. D* **65** 097303.
- [56] Hussain S , Marfatia D , McKay D W and Seckel D, 2006 [hep-ph/0606246].
- [57] DeYoung T, Razzaque S and Cowen D F, 2006 [astro-ph/0608486].
- [58] Bottai S and Perrone L, 2001 *Nucl. Instrum. Meth. A* **459** 319. [hep-ex/0001018].
- [59] Barbot C, Drees M , Halzen F and Hooper D, 2003 *Phys. Lett. B* **555** 22.
- [60] Ishihara A (IceCube Collaboration), 2006 *IceCube projects and its EHE physics capability*, Proceedings of CRIS06, Catania (Italy), to appear in *Nucl. Phys. Proc. Suppl.*
- [61] Learned J G and Pakvasa S, 1995 *Astropart. Phys.* **3** 267.